



Synthesis and electrical properties solid solution of the (1-x)BiO_{1.5}-(x/4)Nb₂Te₂O₉ (x=0.1, 0.2) type δ -Bi₂O₃

L. Loubbidi^{*1}, A. Chagraoui¹, S. Villain², L. Bourja¹, B. Orayech³,
O. Ait Sidi Ahmed¹, A. Moussaoui¹, A. Tairi¹

¹ Laboratoire de Physico-Chimie des Matériaux Appliqués (LPCMA), Faculté des Sciences Ben M'Sik, Université Hassan II- Casablanca, Maroc.

² Avenue de l'université Toulon Var B.P 20132, Laboratoire IM2NP, Bâtiment R83957, La garde CEDEX, Toulon, France.

³ CIC Energigune, Parque Tecnológico, C/ Albert Einstein, 48, 01510 Miñano (Álava), Spain.

*Corresponding Author. E-mail: leila.loubbidi@gmail.com

Abstract

Polycrystalline samples of (1-x)BiO_{1.5}-(x/4)Nb₂Te₂O₉ (x=0.1, 0.2) type δ -Bi₂O₃ were synthesized by a solid reaction and characterized by X ray diffraction. The electrical properties of this new phase were studied using electrical impedance spectroscopy in the temperature range from 200°C to 700°C. Various impedance model including constant phase element and Warburg impedances have been used to interpret the Nyquist representations of electrical analyses. The electrical conductivity was determined to be 1.88165.10⁻³ Scm⁻¹ for x=0.1 and 1.14874.10⁻⁵ Scm⁻¹ for x=0.2 at the temperature 700°C. The activity energy determinate by Arrhenius equation is 0.52eV and 0.48eV for x=0.1 and x=0.2 respectively.

Keywords: Electrical impedance spectroscopy, Nyquist representations, Ionic conduction, δ -Bi₂O₃.

Introduction

The oxygen deficient fluorite of δ -Bi₂O₃ is stable between 730°C and its melting point 825°C [1]. The stability at room temperature can be observed in particular by substituting Bi³⁺ with different mono to hexavalent cations in oxide such as Nb₂O₅, Ta₂O₅, V₂O₅, WO₃, Y₂O₃ and rare earth oxides (Sm to Lu, including Y). This work has been comprehensively reviewed [2, 3]. It is also possible to use a combination of metal oxides called double doping, examples include the ternary systems Bi-Er-Nb [4], Bi-Er-W [5], Bi-Ca-Pb [6] and Bi-Nb-Te [7].

The extensive investigations of δ -Bi₂O₃ solid solutions are motivated by the fact that these materials exhibit very high oxide-ion conductivity [8], providing useful properties for its application in solid oxide fuel, gas sensors... [9, 10].

However, the stability of δ -Bi₂O₃ improvement is usually accompanied by decies in the ionic conductivity resulting in a reduction of the vacancy concentrations.

The structure of δ phase is based on a face centered cubic cation sublattice and can be described as a defective CaF₂ type structure, where a quarter of the available anion sites are vacant [11, 12]. The disorder of the ions in the structure has been investigated in detail [13-15] and it was found that a high concentration of the oxygen vacancies, combined with the high polarizability of the Bi³⁺ 6s² lone electron pairs, increases the oxide ion mobility in this compound [16]. It is the best known oxide ion conductor, with a conductivity of 1 Ω^{-1} cm⁻¹ at 730°C [10].

The present work focused on the electrical studies to obtain more information about conductivity in isolated δ -Bi₂O₃ phase at room temperature. We have used a mixed doping with the aim of combining the stabilizing effect of Nb⁵⁺ cation and the effects of polarizability of Te⁴⁺ ions due to the presence of the important 6s² lone pair.

2. Experimental section

2.1. Sample Elaboration

The compositions (1-x)BiO_{1.5}-(x/4)Nb₂Te₂O₉ type δ -Bi₂O₃ phase have been stabilized with solid state method using the appropriate quantities of high purity oxides powder α -Bi₂O₃, α -TeO₂ and Nb₂O₅. These oxides were

mixed in an agate mortar and then heated at successively higher temperatures (700, 800 and 850°C for 24h) in air with several intermediate grindings and followed by quenching.

2. 2. Electrical analyses

The electrical study was performed using an electrical impedance spectrometer SOLARTRON SI 1260 coupled to an electrical cell operating under air and in the temperature range from 200°C to 700°C. The samples were cylindrical pellets (diameter 12.8±0.1mm, thickness 3±0.05mm) initially compacted at 5kbar under ambient conditions. The pellets were placed between two cylindrical platinum electrodes in a specific cell. A constant pressure was applied to the electrodes via rings. The cell was placed in a furnace operating at up to 700°C. The electrical analyses were carried out in the frequency range ($\omega=2\pi\nu$) 10^{-3} to 10^6 , with an alternating current associated with a maximum voltage of 0.1V. Samples were stabilized for 15 minutes at a fixed temperature. The recording time for the frequency range was of 15 minutes. To ensure thermal stabilization of pellets, the two compositions were subject to two successive measuring cycles (with one temperature rise and drop for two cycles). The final impedance data were chosen during heating mode of the second cycle.

The impedances $Z=Z'+jZ''$ (Z' and Z'' being respectively the real and imaginary components) were represented using Nyquist plots ($X=Z'$, $Y=-Z''$). The software Zview [17] was used to fit the impedance of specific electrical circuit to the Nyquist experimental data (Nyquist representations). The equivalent circuits associated with the two samples were generally based of parallel RC circuit. At low temperature ($\theta<300^\circ\text{C}$) the impedance of such parallel RC circuits is generally expressed as a function of ω as follows:

$$1/Z=1/R+A(j\omega)^n$$

In this expression R is the resistance (associated with the interaction of the Nyquist circle with real Z' axis), the CPE is the constant phase element term A, the frequency ω is expressed in Hz, n is the exponent describing the deviation from the ideal capacitor model and is characteristic of the CPE model. In the case of high temperature results ($\theta>300^\circ\text{C}$), it has been necessary to use a specific modified Warburg model [18-22] having the following form

$$Z_w=R_w \text{Tan}[(jA_w\omega)^{nw}]/(jA_w\omega)^{nw}$$

with R_w as a specific resistance (in Ω), A_w as a specific term depending on diffusion mechanisms, related to the electrode or interface responses, and n being an exponent characteristic of the diffusion process coupled with the simple homogeneity. In the case of pure Warburg diffusion mechanism, this n value should be equal to 0.5. Three circuits placed in series were systematically tested for grain core, grain interface, and electrode contribution. At high temperature, the high frequency impedance for composition $x=0.1$ included an inductance L term. The result of fitting calculations delivered the R, A (CPE) and L parameters, the Warburg characteristics (for high temperature). All observed impedance was normalized using the dimensions of two pellets (surface S and thickness e). As these dimensions were constant for the two compositions ($x=0.1$ and $x=0.2$).

3. Results and discussions

3.1. Nyquist representations

The variation of the values of conductivities has studied at various temperatures and for the two phases ($x=0.1$ and $x=0.2$).

Figures 1a and 1b represent Nyquist plots at 300°C for the compositions $x=0.1$ and $x=0.2$ respectively. We observe the same electrical response; the plots are constituted by two Nyquists circles, the first one associated with grain core conduction while the second one associated with grain boundary. The correspondent model is;

$$Z_1+Z_2 ; 1/Z_1=1/R_1+A_1(j\omega)^{n1} ; 1/Z_2=1/R_2+A_2(j\omega)^{n2}.$$

On figure 2, we have represented a series of Nyquist plots at temperatures above 300°C for the composition $x=0.1$. We have the presence of warburg signal characteristic of diffusion phenomenon and the impedance is given by $Z_3+Z_w ; 1/Z_3=1/R_3+A_3(j\omega)^{n3} ; Z_w=R_w \text{Tan}[(jA_w\omega)^{nw}]/(jA_w\omega)^{nw}$. This phenomenon of polarization in electrodes indicates a good ionic conductivity that corresponds to the oxygen diffusion along to the interface electrode-material

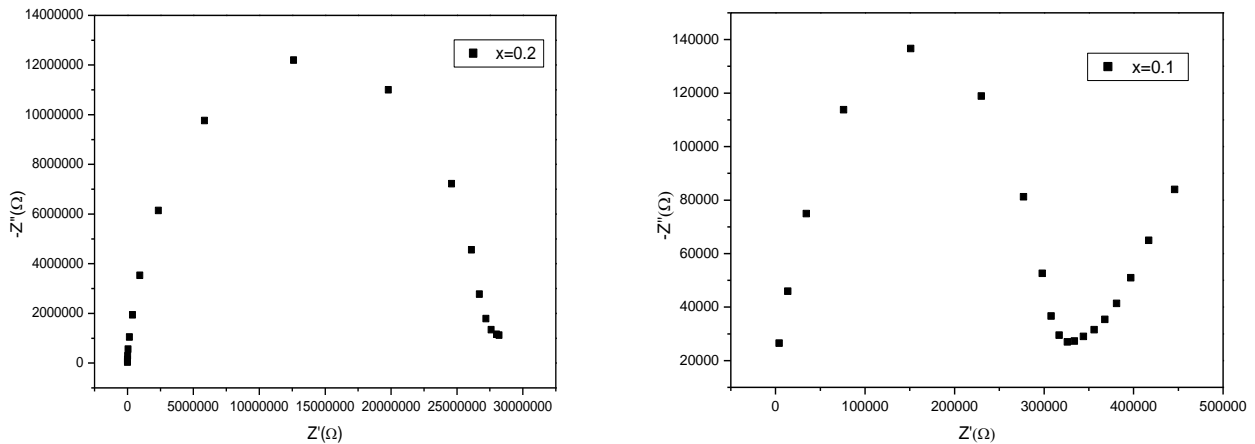


Figure 1: Nyquist plot obtained for composition $x=0.1$ and $x=0.2$ at 300°C

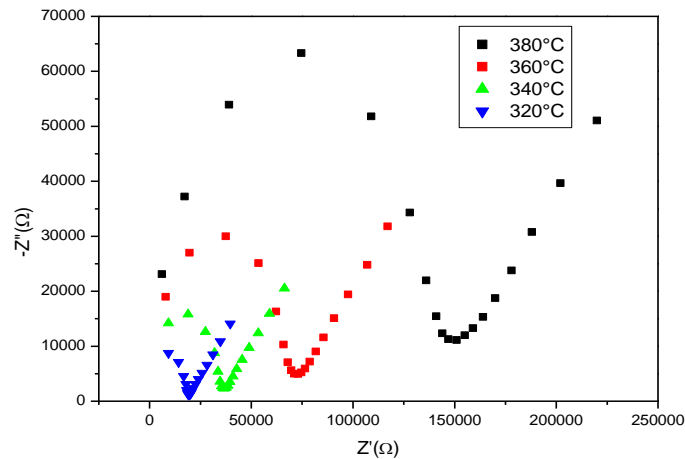


Figure 2: Nyquist plot obtained for composition $x=0.1$ at different temperatures above 300°C

From $T=600^{\circ}\text{C}$, the Nyquist representation for the composition $x=0.1$ is formed by a vertical line which is observed in high frequencies corresponding to negative values of Z'' and a semicircle very flattened in lower frequencies (Figure 3a).

However, for the composition $x = 0.2$, we noticed that significant portion of the first circular arc is not presented on the Nyquist plot in addition of a second semicircle very flattened in lower frequencies (Figure 3b).

3.2. Results of the modeling calculations

On figures 4a, 4b, 4c and 4d, we have reported a part of the results of the modeling calculations with corresponding equivalent circuits. Figure 4a and 4b are relative to composition $x=0.1$ at 300°C and at 400°C respectively. Figure 4c concerns the composition $x=0.2$ at 650°C . Figure 4d is correspondent to the composition $x=0.1$ at 700°C .

3.2. Results of the modeling calculations

On figures 4a, 4b, 4c and 4d, we have reported a part of the results of the modeling calculations with corresponding equivalent circuits. Figure 4a and 4b are relative to composition $x=0.1$ at 300°C and at 400°C respectively. Figure 4c concerns the composition $x=0.2$ at 650°C . Figure 4d is correspondent to the composition $x=0.1$ at 700°C .

Physical parameters were calculated using the equivalent circuits. Tables 1 and 2 include the parameters of the circuits used for the compositions $x = 0.1$ and $x = 0.2$ respectively.

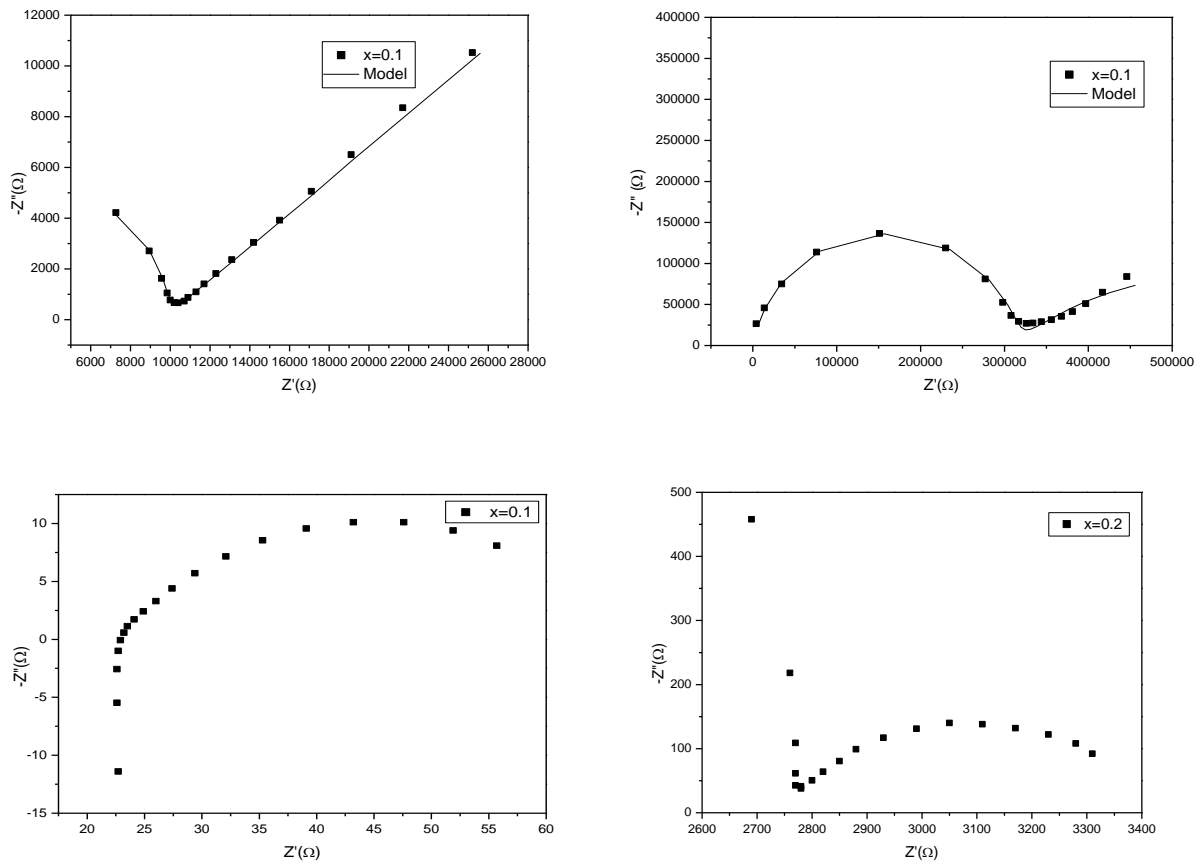


Figure 3: Nyquist plot obtained for composition $x=0.1$ and $x=0.2$ at 700°C

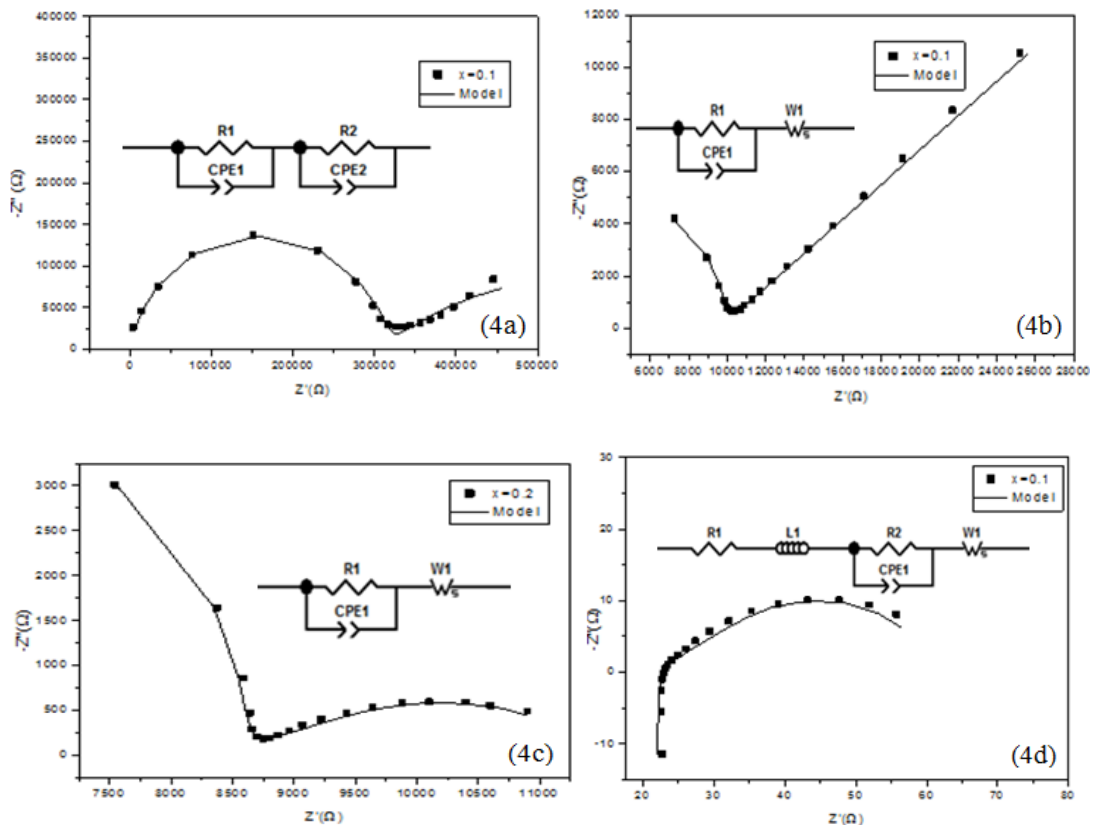


Figure 4: Comparison between experimental results and models.

We noticed that n_1 values decrease, A_1 values increase and the conductivity increase also as a function of the temperature, between 220°C and 300°C. This behavior may have many reasons such as: the increase in the number of charge carriers, the apparition of nonstoichiometric faults, atomic faults and electronic faults and the increase in the mobility of carriers. The R_3 , R_4 and R_w values decrease as the temperature increase.

The values of exponent n are mainly related to the homogeneity (heterogeneity) of the material. The n_1 values associated to the material vary from 0.90 to 0.99, this indicates that the various samples are relatively homogeneous. However, n related to the Warburg varies from 0.26 to 0.5 which is a proof of the contribution of the ionic diffusion.

Table 1: Electrical characteristics of the composition $x=0.1$

Modèle : Z_1+Z_2 $1/Z_1=1/R_1+A_1(j\omega)^{n_1}$; $1/Z_2=1/R_2+A_1(j\omega)^{n_2}$								
T(°C)	$(R_1.10^7)$ (Ω)	$A_1.10^{-11}$	n_1	$(R_2.10^6)$ (Ω)	$A_2.10^{-8}$	n_2		
220	2.4465	2.368	0.92	6.4422	1.0327	0.83		
240	0.6453	2.961	0.91	2.3285	3.6477	0.75		
260	0.20594	3.528	0.90	0.92966	10.458	0.66		
280	0.074868	3.954	0.90	0.47915	32.517	0.55		
Modèle : Z_3+Z_w $1/Z_3=1/R_3+A_1(j\omega)^{n_3}$; $Z_w=R_w \text{Tan}[(jA_w\omega)^{n_w}]/((jA_w\omega)^{n_w})$								
T(°C)	$(R_3.10^3)$ (Ω)	$A_3.10^{-11}$	n_3	$(R_w.10^3)$ (Ω)	A_w	N_w		
320	138.87	3.856	0.92	464.01	5.133	0.36		
340	66.650	3.600	0.93	220.02	2.586	0.35		
360	34.007	3.036	0.94	283.34	16.46	0.36		
380	17.942	2.625	0.96	103.87	2.872	0.36		
400	9.646	2.388	0.97	80.687	3.0387	0.37		
420	5.237	2.755	0.97	55.328	3	0.36		
440	2.970	2.754	0.98	19.821	0.5	0.36		
460	1.783	3.3	0.98	12.483	0.36	0.37		
480	1.082	3.963	0.98	7.516	0.25	0.37		
500	0.6657	4.551	0.97	4.917	0.24	0.35		
510	0.526	4.466	0.91	3.96	0.23	0.34		
520	0.4396	5.162	0.89	3.156	0.18	0.35		
530	0.3732	5.90	0.99	2.414	0.12	0.37		
540	0.3087	6.3	0.98	1.906	0.1	0.37		
550	0.2577	7	0.98	1.519	0.085	0.37		
560	0.1995	7.6	0.89	1.319	0.13	0.32		
570	0.1837	8	0.98	0.9524	0.06	0.37		
580	0.1573	8.7	0.99	0.7494	0.05	0.37		
590	0.1347	9.2	0.98	0.6265	0.053	0.36		
600	0.120	9.7	0.99	0.4861	0.04	0.38		
Modèle : $Z_4+Z_L+Z_w$ $1/Z_4=R_4+JL\omega$; $Z_w=R_w \text{Tan}[(jA_w\omega)^{n_w}]/((jA_w\omega)^{n_w})$								
T(°C)	$(R_4.10^2)$ (Ω)	$L_4.10^{-6}$	(R_2) (Ω)	$A_2.10^{-7}$	n_2	$(R_w.10^2)$ (Ω)	A_w	n_w
610	0.756	2.8401	29	1	0.67	3.779	0.032171	0.38
620	0.6873	3.077	22.44	2.011	0.68	2.916	0.02828	0.38
630	0.58	3.2961	21.48	3.4	0.67	226.6	0.025325	0.38
640	0.6335	2.7048	3.207	4	0.7	187.1	0.030228	0.35
650	0.5544	2.6937	2	4.5	0.72	140.3	0.023696	0.36
660	0.4637	2.754	1.7	5	0.68	107.8	0.021834	0.36
670	0.3814	2.834	1.2	5.6	0.67	0.8259	0.021235	0.36
680	0.3074	2.9134	0.96	6	0.67	0.634	0.022508	0.36
690	0.2479	3.0156	0.8	67	0.68	0.5103	0.031881	0.34
700	0.2065	3.0251	0.73	70	0.68	0.4061	0.037965	0.34

Table 2: Electrical characteristics of the composition x=0.2

Modèle : Z_1+Z_2 $1/Z_1=1/R_1+A1(j\omega)^{n_1}$; $1/Z_2=1/R_2+A1(j\omega)^{n_2}$						
T(°C)	$(R_1 \cdot 10^7) (\Omega)$	$A_1 \cdot 10^{-11}$	n_1	$(R_2 \cdot 10^5) (\Omega)$	$A_2 \cdot 10^{-8}$	n_2
300	2.6861	1.52	0.94	35.373	5.702	0.7
320	1.2895	1.644	0.94	11.40	6.2951	0.88
340	0.63866	1.756	0.94	5.8338	9.9513	0.89
360	0.33986	1.884	0.93	3.4883	2.1831	0.8
Modèle : Z_3+Z_w $1/Z_3=1/R_3+A1(j\omega)^{n_3}$; $Z_w=R_w \tan[(jA_w\omega)^{n_w}]/(jA_w\omega)^{n_w}$						
T(°C)	$(R_3 \cdot 10^3) (\Omega)$	$A_3 \cdot 10^{-11}$	n_3	$(R_w \cdot 10^3) (\Omega)$	A_w	n_w
380	1939.3	1.953	0.93	221.280	0.10484	0.5
400	1194.5	2.078	0.93	1.749	0.083226	0.5
420	749.290	2.071	0.93	154.34	0.074994	0.47
440	477.800	2.069	0.94	119.39	0.09772	0.43
460	309.680	2.001	0.94	104.630	0.13752	0.38
480	204.970	1.917	0.95	85.141	0.18123	0.34
500	138.010	1.842	0.95	69.103	0.29101	0.31
510	115.230	1.822	0.95	59.761	0.29164	0.31
520	96.991	1.759	0.96	52.335	0.33118	0.29
530	81.351	1.735	0.96	45.039	0.36506	0.29
540	67.997	1.557	0.97	38.795	0.43659	0.27
550	56.772	1.486	0.97	32.892	0.47882	0.27
560	47.667	1.445	0.97	26.840	0.44301	0.27
570	39.941	1.340	0.98	23.051	0.5264	0.26
580	33.410	1.272	0.99	18.444	0.43453	0.26
590	27.893	1.254	0.99	14.435	0.30406	0.26
600	23.010	1.094	0.99	12.615	0.38971	0.24
610	19.308	1.542	0.98	8.761	0.16618	0.27
620	15.884	1.304	0.99	6.603	0.11249	0.27
630	12.897	1.061	0.99	5.319	0.10089	0.27
640	10.423	63.58	0.99	4.131	0.079723	0.26
650	8.421	63.58	0.99	3.120	0.057914	0.26
660	6.801	54.32	0.99	2.355	0.047154	0.27
670	5.443	20.61	0.99	1.780	0.039601	0.27
680	4.348	48.45	0.99	1.315	0.031328	0.27
690	3.417	44.39	0.99	0.9755	0.028519	0.27
700	2.706	50.44	0.99	0.6936	0.020691	0.28

3.3. Arrhenius Law

The conductivity follows the Arrhenius-law [23,24] :

$$\sigma = \sigma_0 \exp(-E_a/RT)$$

Where σ_0 , R and E_a denote the pre-exponential factor, the Boltzmann constant $R = 8,314 \text{ J.K}^{-1}\text{mol}^{-1}$, the activation energy, respectively.

Figures 5a and 5b give the Arrhenius plots ($\log \sigma$ (in Scm^{-1}) versus $1000/T$ (in K^{-1})) for $x=0.1$ and $x=0.2$ respectively.

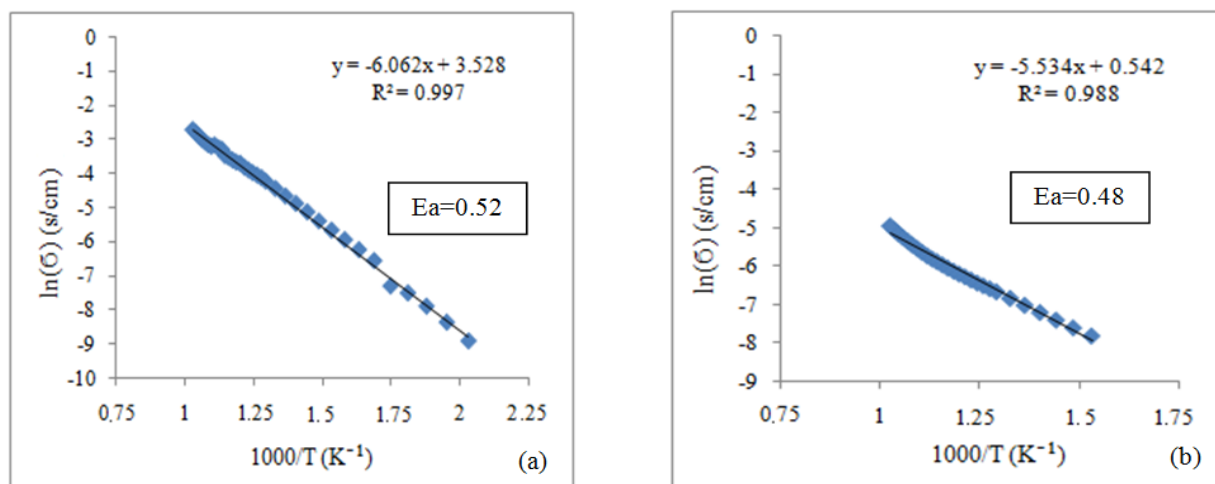


Figure 5: Arrhenius plots for x=0.1(a) and x=0.2(b)

Conclusion

A new phase $(1-x)\text{BiO}_{1.5}-(x/4)\text{Nb}_2\text{Te}_2\text{O}_9$ ($x=0.1$, $x=0.2$) isotype to $\delta\text{-Bi}_2\text{O}_3$ has been stabilized at room temperature [7]. Electrical studies of these two compositions ($x=0.1$ and $x=0.2$) show that the highest conductivity appears at the minimum doping concentrations, that might be explain by the decrease in the vacancies into the structure.

Nyquist diagram analysis have required the use of complex model type Warburg, these models were used to argue the ionic diffusion at interfaces which confirms the predominance of the ionic conduction compared to the electronic conduction in the system studied.

References

1. Helfen A., Merkourakis S., Wang G., Walls M. G., Roy E., Yu-Zhang K., Leprince-Wang Y., *Solid State Ionics* 176 (2005) 629.
2. Sammes N. M., Tompsett G. A., Näfe H., and Aldinger F., *J. Eur.Ceram. Soc.* 19 (1999) 1801.
3. Drache M., Roussel P., and Wignacourt J.-P. *Chem. Rev.* 107 (2007) 80.
4. Chou T., Liu L., Wen-cheg J.w., *J. Eur.Ceram. Soc.* 31 (2011) 3087.
5. Watanabe A., and Sekita M., *Solid State Ion.* 176 (2005) 2429.
6. Drache M., Conflant P., and Boivin J. C., *Solid State Ion.* 57 (1992) 245.
7. Loubbidi L., Chagraoui A., Orayech B., Moussaoui A., Tairi A., Ahmed O. A. S., Igartua J., and Menichi A., *International Journal of Advanced Scientific and Technical Research*, 6 (2014) 1.
8. West A. R., *Basic Solid State Chemistry*, 2nd ed., Wiley, Chichester, (2004) 345.
9. Shuk P., Wiemhofer H. -D., Guth U., Gopel W., Greenblatt M., *Solid State Ionics* 89 (1996) 179.
10. Boivin J. C., Mairesse G., *Chem. Mater.* 10 (1998) 2870.
11. Harwig H. A., *Z. Anorg. Allg. Chem.* 444 (1978) 151.
12. Gattow G., Schröder H., *Z. Anorg. Allg. Chem.* 318 (1962) 176.
13. Kashida S., Nakamura K., *Philos. Mag. Lett.* 73 (1996) 279.
14. Pirnat U., Valant M., Jančar B., Suvorov D., *Chem. Mater.* 17 (2005) 5155.
15. Valant M., Jančar B., Pirnat U., Suvorov D., *J. Eur. Ceram. Soc.* 25 (2005) 2829.
16. Yashima M., Ishimura D., *Chem. Phys. Lett.* 378 (2003) 395.
17. Johnson D., Zview, Impedance software, Version 2.1a, Scribner Associates Inc, (1990–1998).
18. Maria Thompson, *PhD thesis, the College of Engineering and Physical Sciences of the University of Birmingham*, (2010).
19. Lamia Bourja, *PhD thesis, l'Université Ibn Zohr d'Agadir et l'Université du Sud-Toulon-Var*, (2011).
20. Macdonald J. R., *Electrochimica Acta*, 35 (1990) 1483.
21. Barsoukov E., Macdonald J. R., *Impedance Spectroscopy, Theory, Experiment, and Applications*, New Jersey, USA, 2nd edition, (2005) 264.
22. Ho C., Raistrick I. D., Huggins R. A., *Journal of the Electrochemical Society*, 127, (1980) 343.
23. Mogensen M., Sammes N. M., Tompsett G. A., *Journal of Solid State Ionics*, 129 (2000) 63.
24. Suzuki T., Kosacki I., Anderson H. U., *Journal of Solid State Ionics*, 151 (2002) 111.

(2015) ; <http://www.jmaterenvirosci.com>